ELSEVIER

Polymer 43 (2002) 319–327

polymer

www.elsevier.com/locate/polymer

Nanoindentation and nanoscratch testing of uniaxially and biaxially drawn poly(ethylene terephthalate) film

B.D. Beake[a,*], G.J. Leggett[b]

[a]*Micro Materials Ltd, Unit 3, The Byre, Wrexham Technology Park, Wrexham LL13 7YP, UK*
[b]*Department of Chemistry, The University of Manchester, Institute of Science and Technology, P.O. Box 88, Manchester M60 1QD, UK*

Received 12 January 2001; received in revised form 3 August 2001; accepted 21 August 2001

Abstract

Nanoindentation and nanoscratch testing have revealed large differences in nanomechanical behaviour on uniaxially and biaxially drawn poly(ethylene terephthalate) films. Differences can be ascribed to the processing history of the film. The biaxial material exhibited significantly higher hardness and elastic modulus than the uniaxial film, presumably due to increased crystallinity from the second draw. The biaxially drawn material was also less susceptible to creep deformation. The plasticity index, the ratio of the dissipated energy to the total indentation energy, was greater on the uniaxial film, indicating that it exhibits less plastic deformation than the biaxially stretched film. The differences in processing also affected the resistance of the films to nanoscratching wear. The wear resistance of the films correlated with the ratio of the hardness to the modulus.

Keywords: Poly(ethylene terephthalate); Nanoindentation; Melinex

1. Introduction

Surface and near-surface mechanical properties of thin films and coatings can be critical to their final performance. The rapidly expanding field of depth-sensing nanoindentation provides a quantitative method for mapping the mechanical properties, such as hardness and elastic modulus, of the surface/near-surface region [1–3]. Quantification is possible through the use of diamond indenters with well-defined tip geometry [2–6], combined with established models for determining the mechanical properties from the measured data. Nanoindentation has been employed extensively to characterise the mechanical properties of a wide range of hard coatings and surface-modified layers [7–14]. The principle behind nanoindentation is similar to microhardness testing, which employs greater applied load so that the residual indent can be measured optically.

Microhardness testing has provided a wealth of valuable quantitative data regarding deformation processes occurring in semicrystalline polymers such as poly(ethylene terephthalate) (PET) [15], poly(aryl-ether-ether-ketone) (PEEK) [16] poly(propylene) [17] poly(ethylene) [18], elastomers, such as polyisobutadiene rubber [16], and amorphous polymers such as poly(methyl methacrylate) (PMMA) [16,19], and many other systems including polymer blends, copolymers and composites [20,21]. It has been shown that when all components in a multi-phase system have a glass transition (T_g) above room temperature, the microhardness obeys the additivity law, the total measured hardness being the sum of the mass fractions of the hardness of the individual components [21]. It is therefore possible to utilise microhardness measurements to determine the mechanical properties of components and phases, which are not accessible to direct measurement. Microhardness measurements can also be used to detect T_g by following hardness as a function of temperature. Fakirov and co-workers determined a linear relationship between hardness and temperature on a wide range of polymers, including PS, PMMA, PET, PC [22]. Variations in polymer microhardness have been correlated to differences in crystallinity [23,24], molecular weight [24], cohesive energy density [25], microstructure [26], elastic modulus [18] and yield stress [27].

Despite the insights which microhardness testing has provided, far fewer studies of the nanoscale indentation of polymeric materials have been reported [1,15,21,28–32], presumably due to the time-dependent mechanical behaviour which can complicate the interpretation of the results.

In 1990, Ion and co-workers investigated the indentation behaviour of undrawn and uniaxially drawn PET film [28],

* Corresponding author. Tel.: +44-1978-261615; fax: +44-1978-356966.
E-mail address: ben.beake@virgin.net (B.D. Beake).

0032-3861/02/$ - see front matter
PII: S0032-3861(01)00600-0

and found clear differences in their hardness and elastic properties, although exact values of their hardness were not reported. Briscoe and co-workers have shown recently that with newer data analysis methods [29], such as that proposed by Oliver and Pharr [3], it is possible to obtain reliable values of the hardness and modulus.

Flores and Baltà Calleja, and Briscoe and co-workers have shown that hardness measurements with the imaging (microhardness) and compliance (depth-sensing indentation) techniques are in good agreement in the micron regime for amorphous PET [15] and PMMA [16] films.

In the present work, we build on these earlier studies, and report (i) a systematic nanoindentation study of oriented PET film and (ii) nano/microscratching wear testing of the PET film. Oriented PET film has been subject to extensive characterisation at the macroscale [33,34] and the nanoscale [35,36], and therefore is an ideal material to investigate the applicability of depth-sensing indentation to the mechanical characterisation of polymeric materials at the nano/microscale.

In the indentation study, we investigate the effect of film processing history, and experimental parameters, such as loading and unloading rate, hold time at peak load, plastic depth, on the mechanical properties (hardness, modulus, plasticity index) of the film. The relationship between the indentation response and the results of the scratching wear tests has been investigated. We were interested to determine whether there was a direct correlation between the film hardness and its wear resistance, or whether the microscale wear resistance of the films is a function of the hardness/modulus ratio, as has been recently suggested [37,38].

2. Experimental

2.1. Materials

The PET films used in this study were a biaxially drawn PET and an experimental uniaxially drawn material, with a draw ratio of 3.3. Both were obtained from ICI (Wilton, UK) and used as received. For the biaxial material, the draw ratios for the first draw in the machine direction and the subsequent transverse draw were both set approximately equal (~3.2) so that the their product was ~10 [33]. Both films were additive-free and of very low surface roughness [35].

2.2. Nanoindentation

A NanoTest System manufactured by Micro Materials was used for the nanoindentation testing. Details of the specifications of the instrument have been published previously [1,21]. The NanoTest is a pendulum-based depth-sensing system, with the sample mounted vertically and the load applied electromagnetically. Current in the coil causes the pendulum to rotate on its frictionless pivot so that the diamond probe penetrates the film surface. Test probe displacement is measured with a parallel plate capacitor with sub-nm resolution.

A Berkovich (three-sided pyramidal) diamond indenter was used for all the indentation testing. In view of the rounding of the indenter at the tip, it is necessary to determine the area function of the indenter to obtain meaningful values of hardness and modulus. The area function for the diamond, which is used to determine the contact area for a given depth, was calibrated by indentations to different depths into fused quartz (load range: 0.5–200 mN). Fused quartz is an isotropic material used as a calibration standard by the nanoindentation community because its hardness and elastic modulus do not vary significantly with indentation depth. The area function for the diamond used in this work was $A = 21.8h_c^2 + 2100h_c$, where h_c is the contact depth. For comparison, the area function of an ideal Berkovich diamond is $A = 24.5h_c^2$. Fused quartz was also used to determine the instrument (frame) compliance, which was 0.48 nm/mN for the instrument used in this work. The measured depth is adjusted for the effect of instrument compliance in the instrument software. The indentation loading and unloading rates were set equal in all the tests. The normal experimental conditions were 0.1–5 mN applied load, initial (contact) load 0.03 mN, loading rate = unloading rate = 0.06 mN s^{-1}, with a 60 s holding period at peak load. To determine the importance of these parameters on the measured hardness and modulus, experiments were performed where one of these parameters was varied while keeping the others constant. Indentations were load-controlled (constant velocity) and repeated at least five times on different regions of the film surface.

2.3. Multi-pass nanoscratch testing

A NanoTest System was also used for the nanoscratch testing. Multi-pass scratch tests over the same region of the film surface can be scheduled in the instrument software. To investigate the wear resistance of the PET films, schedules of repeat alternate 'off-load' topography scans and 'on-load' scratch tests were set up. A 25 μm radius spherical diamond was used as the probe in all the tests. In the initial topography scan, a small load of 0.1 mN was applied to the probe and the sample scanned for 100 μm at 0.5 μm s^{-1}, and automatically moved back to its starting position for the scratch test. In the scratch test, the probe is moved along the same track for 10 μm (this can aid levelling of data if necessary) before the applied load is ramped at 0.02 mN s^{-1} to the pre-set maximum load 1 mN, at 35 μm. For the remainder of the test (35–100 μm), the probe scratched the film surface at a constant load of 1 mN. After automatically moving the sample back to its starting position, the process was repeated (total topographic scans 4, scratches 3), before a final topography scan (at 0.1 mN applied load).

2.4. Indentation data analysis

A schematic of a loading–unloading cycle is shown in

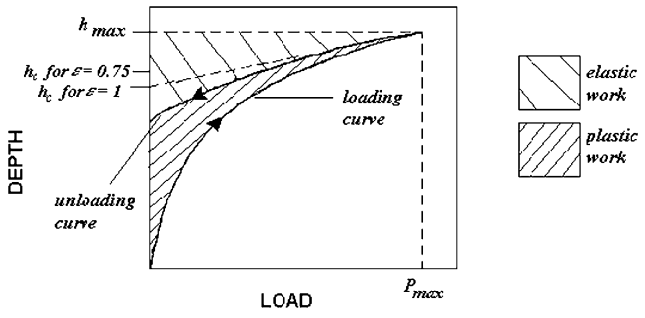

Fig. 1. Schematic representation of loading–unloading cycle.

Fig. 1. For clarity creep occurring during the hold period at maximum load has been omitted. It is possible to define several different plasticity indices. Following Briscoe and co-workers [29], we use the plasticity index, I_P, which is defined as the ratio of the plastic (or dissipated) energy, ψ_p, the area between the loading and unloading curves, to the elastic (or recovered) energy, ψ_e, the area bounded by the unloading curve, the maximum depth (h_{max}) and the maximum and minimum applied load as shown in Fig. 1 [29,39].

$$I_P = \psi_p/(\psi_p + \psi_e) \quad (1)$$

The depth vs. load raw unloading data was fitted to a power-law function, as originally proposed by Oliver and Pharr [3], to determine the hardness and modulus of the film, after correction for the effects of instrument compliance (Eq. (2))

$$\text{Contact compliance } C = \text{total compliance } (C_t) - \text{machine compliance } (C_m) \quad (2)$$

where contact compliance = 1/contact stiffness. The power-law function has the form

$$P = a(h - h_f)^m \quad (3)$$

where P is the load, $(h - h_f)$ is the elastic displacement, and a and m are material constants. The indenter contact (or plastic) depth, h_c, is determined from the expression:

$$h_c = h_{max} - \varepsilon(CP_{max}) \quad (4)$$

where C is the contact compliance equal to the tangent at maximum load (P_{max}). The value of ε is a function of the indenter geometry and depends on the pressure distribution that is established after the plastic deformation. For flat punch indenter ε is 1, whereas for a Berkovich indenter, as used in this study, ε is taken as 0.75 since most indenters have a rounded tip. The plastic depths corresponding to these indenter geometries are shown in Fig. 1. The diamond area function $A(h_c)$ was determined separately from indentations into fused quartz.

The hardness (H) is determined from the peak load (P_{max}) and the projected area of contact, A:

$$H = P_{max}/A \quad (5)$$

To obtain the elastic modulus, the unloading portion of the depth–load curve is analysed according to a relation which depends on the contact area:

$$C = \pi^{0.5}/(2E_r A^{0.5}) \quad (6)$$

where C is the contact compliance and E_r is the reduced modulus defined by

$$1/E_r = (1 - \nu_s^2)/E_s + (1 - \nu_i^2)/E_i \quad (7)$$

where $\nu_s$is the Poisson's ratio for the sample, ν_i, the Poisson's ratio for the indenter (0.07), E_s, the Young's modulus for the sample and E_i, the Young's modulus for the indenter (1141 GPa) [40].

In obtaining accurate hardness and modulus values, it was necessary (particularly for very shallow indentations) to determine the offset in the apparent depth caused by the application of a set finite load to make contact (i.e. a 'zero-error' correction). In all the data reported in this paper, the loading data have been fitted to a power-law function (Eq. (8)) in the instrument software to determine this depth offset, as has been done previously [15,16].

$$P = a(h - h_0)^n \quad (8)$$

where P is the load, h_0, the real depth zero, a, a material parameter and n, the index of the deformation (indentation exponent).

The fit of the loading curve data to this function is very good. Fig. 2 shows a typical power-law fit to a 3 mN indentation into the biaxial film; the fitted curve superimposes virtually exactly over the loading data. When a Berkovich indenter is used, the value of n is often very close to 2 [41–44]. However, deviations from this are known to occur, particularly for polymers (e.g. due to strain-rate effects), and are discussed in more detail in Section 3.

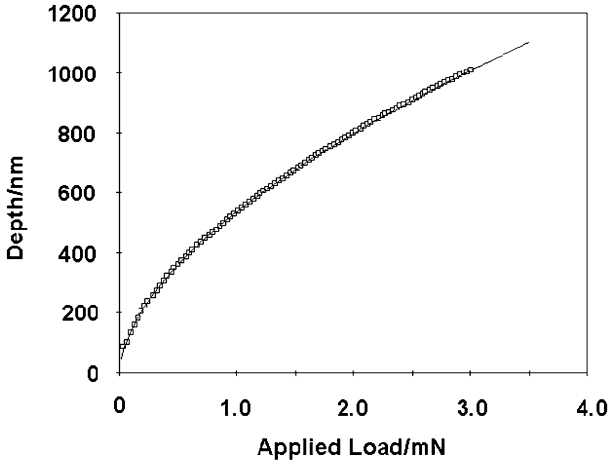

Fig. 2. A 3 mN indent on the biaxial Melinex film showing the power-law fit to the loading data to determine the true depth zero.

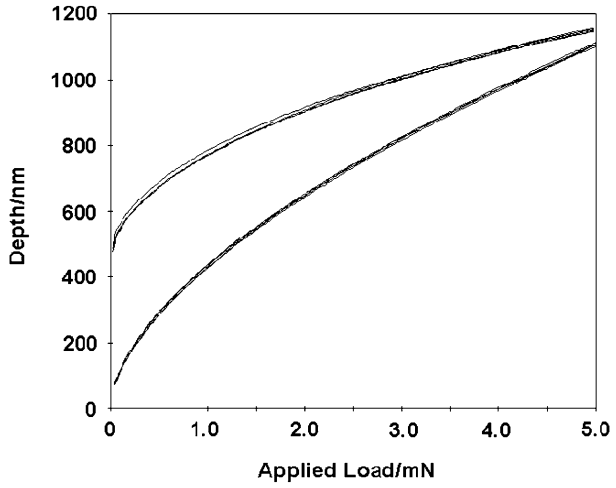

Fig. 3. Five superimposed indentation curves on the biaxial Melinex O film. The indentations were to a maximum applied load of 5 mN at a loading rate 0.06 mN s^{-1} with 60 s hold period at peak load.

3. Results and discussion

3.1. Indentation: general features

Nanoindentation testing can be used as a qualitative tool for investigating polymer film uniformity. The data showed that both the uniaxial and biaxial material were homogeneous films exhibiting mechanically uniform properties from region-to-region across the surface. To illustrate this, Fig. 3 shows load–depth data from five 5 mN indentations spaced 20 μm apart on the surface of the biaxial Melinex 'O' film. The loading–unloading curves superimpose almost exactly, indicating that the film is mechanically homogeneous at the sub-μm scale.

Fig. 4 shows single 3 mN indentations into the biaxial and uniaxial materials. It is immediately clear that the mechanical response of the two polyester films differs considerably despite their identical chemical composition. The maximum indentation depth at peak load is greater on the singly drawn film and there is also a clear difference in the unloading behaviour. In addition, the uniaxial material exhibited almost double the amount of creep deformation during the holding period at maximum load. The hardness and reduced modulus have been determined from these indentation curves using a method originally proposed by Oliver and Pharr which fits a power-law function to the unloading curve [3].

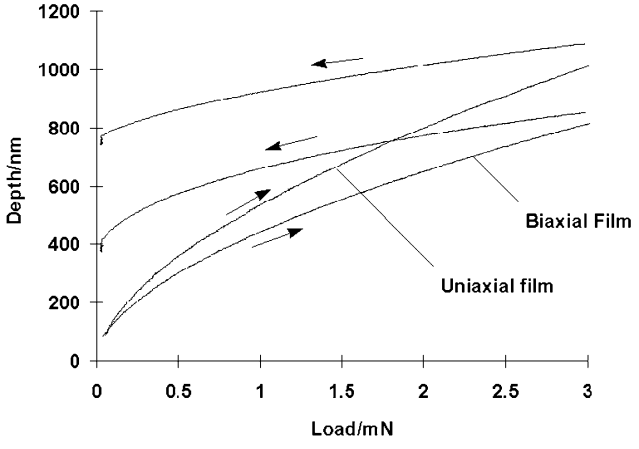

Fig. 4. Indentation curves on biaxial and uniaxial films. The indentations were to a maximum applied load of 3 mN at a loading rate 0.06 mN s^{-1} with 60 s hold period at peak load.

The hardness and reduced modulus determined from the 3 mN indentations in Fig. 4 were 0.252 and 3.55 GPa, respectively on the biaxially oriented film and 0.141 and 2.72 GPa, respectively on the uniaxially oriented film. The biaxial film is ~80% harder and ~30% stiffer. It is interesting to compare the hardness values with those obtained by microhardness measurements on undrawn PET samples. Since, in general, microhardness obeys the additivity law, the total measured hardness can be written as the sum of the hardness of the volume fractions of crystalline and amorphous material:

$$H = w_c H_c + (1 - w_c) H_a \quad (9)$$

where H_c and H_a are the intrinsic microhardness of the crystalline and amorphous phases, respectively, and w_c is the volume fraction of crystalline material (i.e. wt% crystallinity) [21]. The accuracy of this relationship has been tested on several systems, and indeed a linear relationship between H and w_c has been observed on melt-crystallised polypropylene, PET, and nylon 6 annealed at different temperatures [23,24]. Extrapolation of the linear plot of H vs. w_c enabled Vanderdonckt and co-workers to estimate the H values of fully crystalline and completely amorphous PET as 0.400 and 0.120 GPa, respectively [23]. The crystallinity of the biaxial Melinex film is ~45–50% [33,45]. The estimated crystallinity from the nanohardness measurement is ~47% in good agreement with this. The crystallinity of the uniaxial film is ~33%, considerably lower than the biaxial film, due to the absence of the second draw and subsequent heat set. The much lower measured nanohardness is in agreement with this, although a value closer to 0.2 GPa would have been predicted from the microhardness data.

3.2. Creep deformation

Hardness is defined as resistance to permanent deformation. As the film hardness is derived from the contact depth at maximum load, it will be affected by creep deformation occurring during the dwell time at maximum load. In addition, it is known that that if this dwell time is absent, the sample will continue to deform viscoplastically, while the load is being removed, significantly distorting the shape of the unloading curve. This leads to inaccurate values of the modulus as it is determined from the tangent to the slope of the unloading curve at maximum load [15,29,46]. The variation in hardness and modulus with rate of loading and the creep occurring during the holding time has been

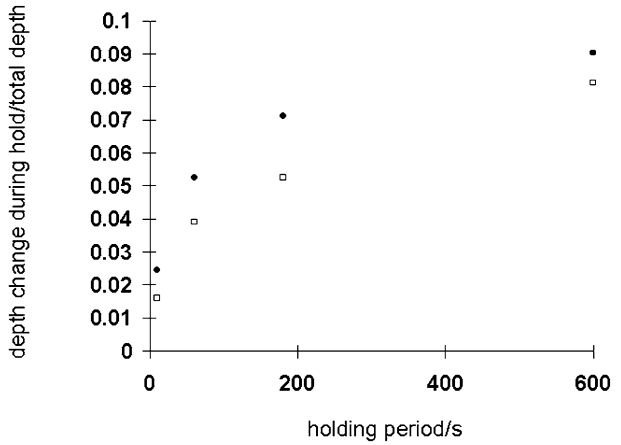

Fig. 5. Creep deformation ratio vs. hold time on biaxial film (squares) and uniaxial film (filled circles). (error bars shown are ±5%).

investigated to determine standard conditions with which to evaluate the influence of processing history and any variation of mechanical properties with depth from the film surface.

Fig. 5 shows how the extent of creep deformation varies slightly with the dwell time at peak load. The ratio of displacement during hold vs. the total displacement was fairly small (~0.04–0.05 at 60 s). Hardness and modulus values obtained from indentations to a peak load of 5 mN at a loading rate 0.06 mN/s, with differing hold periods at peak load are shown in Table 1 (for the biaxial film) and Table 2 (for the uniaxial material). It is clear that there is a small decrease in both quantities as the hold period was extended on both samples.

From the data in Tables 1 and 2, a 60 s dwell time was deemed acceptable for the majority of the experiments, since this is sufficient to reduce significantly the effect of creep on the unloading data, while keeping the overall experimental time to a few min, and not greatly affecting the measured hardness. For comparison, Briscoe and co-workers decided a holding time of 10 s was sufficient to minimise the effects of creep on the unloading data in a previous study of poly(methylmethacrylate) (PMMA), polystyrene (PS), polycarbonate (PC) and ultrahigh molecular weight polyethylene (UHMWPE) [29], and in a ultramicrohardness study on amorphous PET, Flores and

Table 1
Effect of dwell time on hardness and modulus of biaxial film (peak load: 5 mN; loading rate: 0.06 mN s^{-1})

Dwell time (s)	Hardness (GPa)	Reduced modulus (GPa)
10	0.259 ± 0.03[a]	3.11 ± 0.04
60	0.248 ± 0.02	2.96 ± 0.04
180	0.235 ± 0.04	2.91 ± 0.03
600	0.214 ± 0.00	2.91 ± 0.05

[a] The standard error in the mean (from five indentations) is shown as an indication of the reproducibility of the measurements.

Table 2
Effect of dwell time on hardness and modulus of uniaxial film (peak load: 5 mN; loading rate 0.06 mN s^{-1})

Dwell time (s)	Hardness (GPa)	Reduced modulus (GPa)
10	0.139 ± 0.01[a]	2.61 ± 0.02
60	0.132 ± 0.01	2.42 ± 0.01
180	0.125 ± 0.01	2.34 ± 0.01
600	0.119 ± 0.02	2.34 ± 0.02

[a] The standard error in the mean (from five indentations) is shown as an indication of the reproducibility of the measurements.

Baltà Calleja found that although 6 s was acceptable for hardness, longer hold times were preferable for accurate modulus determination [15].

Creep data (depth increase during hold vs. time) were found to follow the general logarithmic creep formula (Eq. (10)), which has recently been used to describe the creep behaviour of glasses, ceramics and thin DLC coatings [46] by nanoindentation.

$$h = A \ln(Bt + 1) \tag{10}$$

where h is the increase in depth at maximum load, t, the time, and A and B, the fitting parameters. Analysis of creep data from repeat indents to 5 mN at 0.06 mN/s gave mean values of A of 30.6 and 18.5 on the uniaxial and biaxial material respectively. Mean values of B were 0.19 and 0.16, respectively.

3.3. Loading rate behaviour

The variation in hardness, modulus and indentation exponent with rate of loading and unloading was examined over the range of loading rate (= unloading rate) of 0.01–1.0 mN s^{-1}, while keeping the holding period constant (60 s) for indentations to a peak load of 5 mN. The indentation exponent (n) determined from the power-law fits to the loading curves (Eq. (8)) was very similar for both films, and

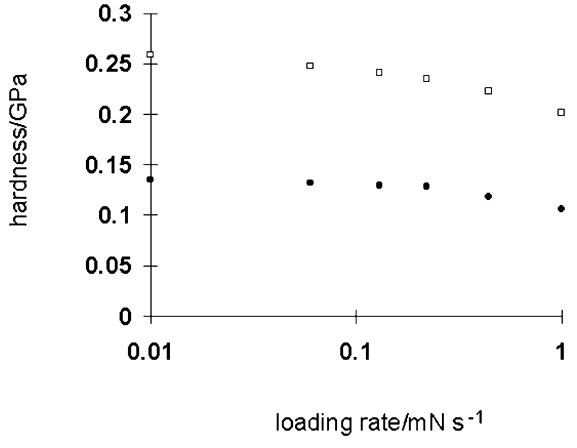

Fig. 6. Variation of hardness with loading rate on both films: biaxial (squares) and uniaxial film (filled circles).

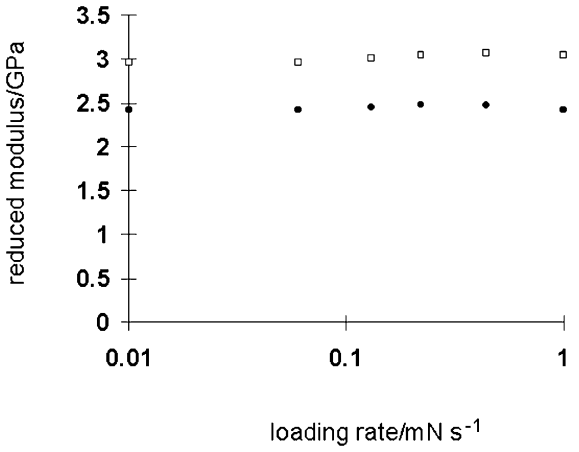

Fig. 7. Variation of reduced modulus with loading rate on both films: biaxial (squares) and uniaxial film (filled circles).

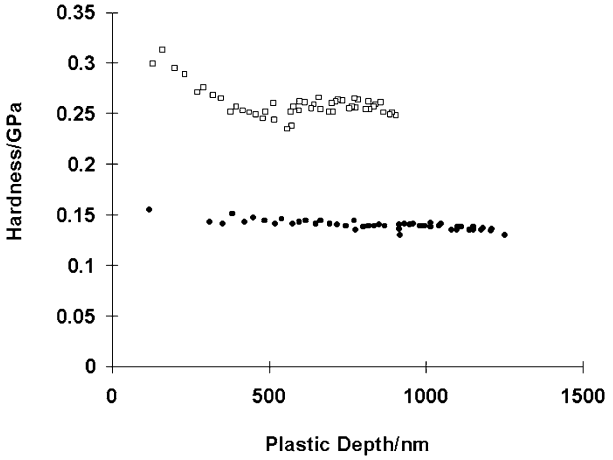

Fig. 8. Variation of hardness with plastic depth on both films: biaxial film (squares) and uniaxial film (filled circles).

varied clearly with loading rate, e.g. $n \sim 1.73$ at 0.01 mN/s, increasing to ~1.87 at 1.0 mN/s. Figs. 6 and 7 illustrate that the hardness and modulus exhibit different trends with changing loading rate. For both materials there is a moderate (~30%) rise in hardness as the loading rate is decreased from 1.0 to 0.01 mN s^{-1}, whereas the modulus is virtually unchanged throughout the whole range. Since the elastic modulus is determined from the slope of the unloading curve, this implies that the recovery is not strongly time-dependent under these experimental conditions. Microhardness measurements on amorphous PET films have previously shown the elastic modulus to be sensitive to the loading rate, increasing by ~20% when the loading rate was increased from 0.47 to 13.2 mN/s, which the authors attributed to increased viscoelastic recovery at the higher loading rates [15]. Increasing the hold time from 6 to 200 s was found to dramatically reduce this effect. This finding supports the choice of experimental conditions employed in this current work (low loading rate together with relatively long hold time) for determination of reliable modulus values.

Interestingly, the ratio of the hardness of the two materials remains constant independent of the loading rate; H(biaxial): H(uniaxial) ~ 0.53. Both materials creep more during the hold period when subjected to more rapid loading and hence have lower hardness, as this is determined from the contact depth immediately before the unloading process. In their 'abrupt loading' tests on undrawn and uniaxial PET films, Ion and co-workers found an increased maximum on-load depth in than in slow-loading experiments [28]. They suggested that viscous flow was occurring at the much higher mean stress involved in the abrupt loading test. In microhardness measurements, no appreciable variation in hardness with loading rate was observed on amorphous PET films by Flores and Baltà Calleja, using a hold time of 6 s and a peak load of 147 mN [15]. In contrast, indentations into PEO [47] and PMMA film [29,48] have revealed a strain-hardening effect.

3.4. Variation of mechanical properties with depth from the film surface

Figs. 8 and 9 show the variation in hardness and modulus with depth, calculated from 50 indentations, at 0.1 mN intervals covering the loading range 0.1–5.0 mN, into each film surface. The loading rate was 0.06 mN/s and the dwell time 60 s in all the tests. Since each point represents a single indent rather than an averaged value, there is some point-to-point variability, though it is very small.

For both materials, Figs. 8 and 9 show a very slight rise in hardness with a more pronounced rise in reduced modulus as the indentation depth decreases. On the uniaxial film, the hardness varied from 0.130 GPa at a plastic depth of 1251 nm to 0.155 GPa at 118 nm. The reduced modulus varied from 2.47 to 4.21 GPa over the same range. On the biaxial film, the hardness varied from 0.248 GPa at a plastic depth of 904 nm to 0.299 GPa at 131 nm. The reduced modulus varied from 3.42 to 5.27 GPa over the same range. The increases in hardness and modulus became more pronounced when indenting to less than 400 nm

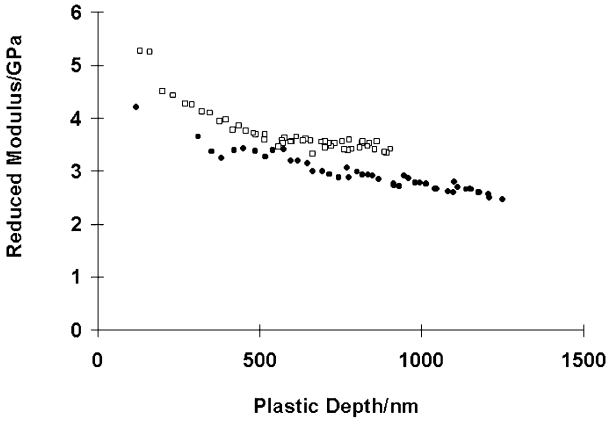

Fig. 9. Variation of reduced modulus with plastic depth on both films: biaxial film (squares) and uniaxial film (filled circles).

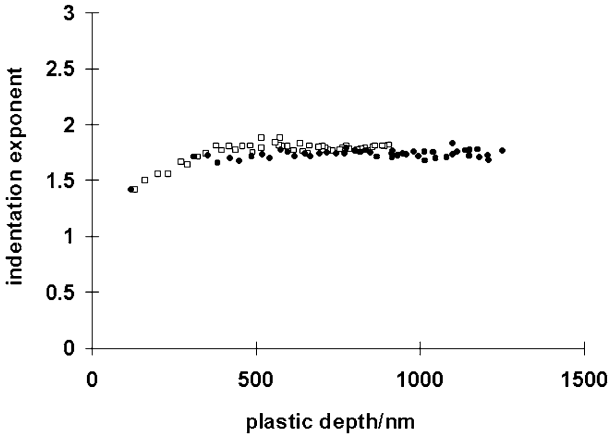

Fig. 10. Variation of indentation exponent with plastic depth on both films: biaxial film (squares) and uniaxial film (filled circles).

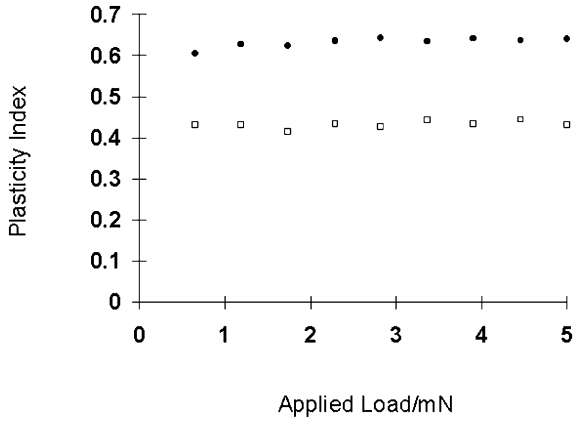

Fig. 11. Variation in plasticity index with maximum applied load between 0.65 and 5.0 mN: biaxial film (squares) and uniaxial film (filled circles). The plastic depths corresponding to these loads were 302–912 nm on the biaxial film and 409–1235 nm on the uniaxial material.

from the film surface. The near constant hardness above 500 nm is agreement with the results of Flores and Baltá Calleja on isotropic PET film [15]. They investigated the variation of hardness with indentation depth on glassy PET by ultramicrohardness testing and found that, once correction for tip defect was made (i.e. an accurate area function for the tip was used), the hardness was essentially independent of depth in the range 0.5–9 μm.

It is interesting to speculate on whether the increase in hardness near to the surface is an indentation size effect, or represents a change in the mechanical properties of the near-surface region due to enhanced crystallinity. On polymers which strain-rate harden, such as PMMA [29,48], increasing near-surface hardness and modulus has been attributed to a strain-rate effect. In a load-controlled (constant velocity) indentation the strain rate will decrease with increasing indentation depth, which is thought responsible for the apparent decrease in hardness with depth [48]. On PET, however, which unlike PMMA does not strain-rate harden, the explanation must be more complex.

Several factors can affect whether the normal relationship [41–44] between load and depth during an indentation (load α depth^2) holds. Deviations from this (i.e. $n \neq 2$) can occur when (i) there is strain rate hardening, (ii) there are viscoelastic effects, (iii) the mechanical properties (hardness and modulus) vary with depth due to a changing crystallinity profile [49]. It is clear that viscoelastic effects are important for PET since n is always less than 2 in our tests. Viscoelastic effects can be also be inferred from the observed variation in the indentation exponent, n, with loading rate.

We have also investigated how the indentation exponent varies with depth at constant loading rate. Fig. 10 shows the variation of the exponent with plastic depth corresponding to the indentations in Figs. 8 and 9. It can be seen that above 500 nm, n is ~1.8 on both the uniaxial and biaxial films, and decreases with depth below about 500 nm. Pollock and co-workers also observed that their values of n, determined by a different procedure, tended to decrease nearer the surface, and that this tendency was increased on drawn PET films [28]. It has previously been suggested that PET films are more crystalline in the near-surface region than in the bulk [45], possibly due to orientation-induced crystallisation [50]. In view of this, the conclusion of Pollock and co-workers [28], that drawing the films has a greater effect of the topmost layers seems reasonable, although clearly, care must be taken in interpreting the near-surface indentation response of viscoelastic-plastic materials.

3.5. Plasticity index

The plasticity index, as defined by Eq. (1), has been calculated in the instrument software without including the displacement (creep deformation) occurring during the hold period. Fig. 11 shows the variation of the plasticity index with applied load for both materials. It is clear that the uniaxial material deforms more plastically than the biaxially stretched Melinex. Interestingly, although there are differences in elastic modulus over the range of applied load, both materials being harder and stiffer nearer the surface, this has relatively little influence on their plasticity.

3.6. Multi-pass nanoscratch testing

Typical results from multi-pass scratch tests are shown in Figs. 12 and 13. It is clear that both surfaces are worn considerably under these conditions. Table 3 summarises the results from five tests. There are clear differences between the samples. The biaxial film exhibits better wear resistance as judged by both on-load total (elastic + plastic) depths and off-load plastic depths after the three scratches. Table 3 also shows that the biaxial film exhibits less plastic deformation than the uniaxial film, having a lower ratio of the plastic to total depth. This mirrors the differences in plasticity index observed in the indentation experiments, although an exact correlation should not be expected due to the differences in indenter shape (and hence contact strain) in the two sets of experiments.

It has been reported that a low E/H ratio is beneficial for

Table 3
Multi-pass scratch test results

Film	Total depth (nm)[a]	Plastic depth (nm)	Ratio of plastic to total depth
Uniaxial	722, 861	367, 488	0.51, 0.57
Biaxial	584, 494, 652	231, 194, 321	0.39, 0.40, 0.49

[a] The total (on-load) and plastic (off-load) depths are taken from the final scratch on each sample.

wear resistance by limiting plastic deformation and promoting elastic deformation [1,37]. If resistance to scratching wear is proportional to H/E, which is closely related to the elastic recovery parameter [1], then we would expect wear to be ~1.6 times greater on the uniaxial film based on the difference in E/H between the two materials determined from indentation measurements (e.g. using the data in Tables 1 and 2). Table 3 shows that (within the precision of the measurements) this was found experimentally.

The surface topography after scratching was quite different on the two samples. A pattern consisting of alternating peaks and troughs was observed in the region after 35 μm scan distance previously scanned at 1 mN constant load, possibly due to a stick-slip process. On the biaxial material, the size of the peaks increases with each subsequent scan. Their wavelength (i.e. peak-to-peak repeat distance of the saw-tooth structure) is significantly greater on the uniaxial film, although the structure is less regular. The sample orientation with respect to the scratching direction was altered between the two sets of experiments on the uniaxial film. The values of the total depth were within 20% of each other, suggesting that film orientation does not greatly effect the resistance of the surface/near-surface region to scratching wear, as has been found in studies of AFM-tip induced wear of the same material [51].

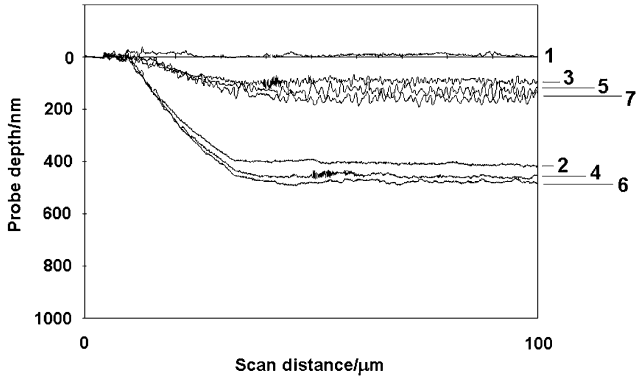

Fig. 12. The evolution of surface damage during a multi-pass scratch test on the biaxial film. The scan direction is from left to right in all 7 scans. Scans 1, 3, 5 and 7 are low-load topography scans, and 2, 4 and 6 are scratch tests.

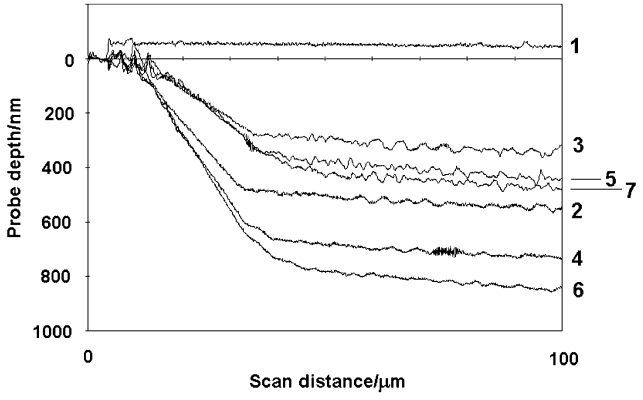

Fig. 13. The evolution of surface damage during a multi-pass scratch test on the uniaxial film. The scan direction is from left to right in all 7 scans. Scans 1, 3, 5 and 7 are low-load topography scans, and 2, 4 and 6 are scratch tests.

4. Conclusions

Nanoindentation and nanoscratch testing have revealed large differences in the mechanical properties of uniaxially and biaxially drawn PET films, which can be ascribed to the differences in processing history of the films. Melinex O, the biaxially drawn material, exhibits significantly higher hardness and elastic modulus than the uniaxial film, presumably due to its higher crystallinity. The biaxial film is also less susceptible to creep deformation. The plasticity index, the ratio of the dissipated energy to the total indentation energy is greater on the uniaxial film, indicating that it exhibits less plastic deformation than the biaxially stretched film. The differences in processing also affect the resistance of the film to nanoscratching wear. The wear resistance of the films correlated with the ratio of the hardness to the modulus.

Acknowledgements

The authors would like to acknowledge Dr D.H. MacKerron of ICI Films Division, Wilton, UK, for kindly supplying us with experimental uniaxially oriented film and information on the conditions used to prepare it, and Prof. D. Briggs for supplying samples of the biaxial Melinex O film. Dr F. Gao (Nottingham Trent University) and Dr Ir. J.M.J. den Toonder (Philips Research Laboratories, Eindhoven) are both thanked for very helpful discussions.

References

[1] Pollock HM. Nanoindentation. ASM Handbook 1992;18:419–29.

[2] Doerner MF, Nix WD. J Mater Res 1986;1:601–9.
[3] Oliver WC, Pharr GM. J Mater Res 1992;7:1564–83.
[4] Jennett NM, Meneve J. Proc MRS Symp 1998;522:239–44.
[5] Hermann K, Jennett NM, Wegener W, Meneve J, Hasche K, Seemann R. Thin Solid Films 2000:377–8, see also p. 394–400.
[6] Jennett NM, Shafirstein G, Saunders SRJ. Hardness testing in theory and practice. Dusseldorf: VDI Berichte 1194, VDI-Verlag GmbH, 1995. p. 201–10.
[7] Pivin JC. Thin Solid Films 1993;229:83–92.
[8] Brontzen FR. Int Mater Rev 1994;39:24–45.
[9] Meneve JL, Smith JF, Jennett NM, Saunders SR. Appl Surf Sci 1996;100/101:64–68.
[10] Zheng S, Sun Y, Bell T, Smith JF. Proceedings of the 4th European Conference on Advanced Materials and Processes, Venice, Italy, September 1995. AIM, 1995 p. 177.
[11] Zheng S, Sun Y, Bloyce A, Bell T. Mater Man Proc 1995;10:815–24.
[12] Martínez E, Polo MC, Pascual E, Esteve J. Diam Relat Mater 1999;8:563–6.
[13] Lousa A, Martínez E, Esteve J, Pascual E. Thin Solid Films 1999:355–6, see also p. 210–3.
[14] Esteve J, Martínez E, Lousa A, Montalà F, Carreras LL. Surf Coat Technol 2000:133–4, see also p. 314–8.
[15] Flores A, Baltá Calleja FJ. Phil Mag A 1998;78:1283–97.
[16] Briscoe BJ, Sebastian KS, Sinha SK. Phil Mag A 1996;74:1159–69.
[17] Martínez-Salazar J, García Tijero JM, Baltá Calleja FJ. J Mater Sci 1988;23:862.
[18] Flores A, Baltá Calleja FJ, Attenburrow GE, Bassett DC. Polymer 2000;41:5431–5.
[19] Briscoe BJ, Sebastian KS. Proc R Soc A 1996;452:439–57.
[20] Baltá Calleja FJ. Adv Polym Sci 1985;66:117.
[21] Baltá Calleja FJ, Fakirov S. Microhardness of polymers. Cambridge, UK: Cambridge University Press, 2000.
[22] Fakirov S, Baltá Calleja FJ, Krumova M. J Polym Sci Polym Phys 1999;37:1413–9.
[23] Krumova M, Fakirov S, Baltá Calleja FJ, Evstatiev M. J Mater Sci 1998;33:2857–68.
[24] Vanderdockt C, Krumova M, Baltá Calleja FJ, Zachmann HG, Fakirov S. Colloid Polym Sci 1998;276:138–43.
[25] Martínez-Salazar J, García Peña J, Baltá Calleja FJ. Polym Commun 1985;26:57.
[26] Santa Cruz C, Baltá Calleja FJ, Zachmann HG, Stibeck N, Asano T. J Polym Sci B 1991:819–24.
[27] Santa Cruz C, Baltá Calleja FJ, Asano T, Ward IM. Phil Mag 1993;68:209.
[28] Ion RH, Pollock HM, Roques-Carmes C. J Mater Sci 1990;25:1444–54.
[29] Briscoe BJ, Fiori L, Pelillo E. J Phys D 1998;31:2395–405.
[30] Dwyer-Joyce RS, Ushijima Y, Murakami Y, Shibuta R. Tribol Int 1998;31:525–30.
[31] Benítez F, Martínez E, Galán M, Serrat J, Esteve J. Surf Coat Technol 2000;215:383–7.
[32] VanLandingham MR, Villarrubia JS, Guthrie WF, Meyers GF. Macromol Symp 2001;167:15–43.
[33] Mills PJ. In: Ward IM, editor. Structure and properties of oriented polymers, 2nd ed. London: Chapman & Hall, 1997. p. 423–46.
[34] Heffelfinger CJ, Knox KL. In: Sweeting OJ, editor. The science and technology of polymer films, vol. II. New York: Wiley-Interscience, 1971. p. 587–639.
[35] Beake BD, Ling JSG, Leggett GJ. Polymer 2000;41:2241–8.
[36] Beake BD, Brewer NJ, Leggett GJ. Macromol Symp 2001;167:101–15.
[37] Dong H, Bell T. Surf Coat Technol 1999;111:29–40.
[38] Jardret V, Zahouani H, Loubet JL, Mathia TG. Wear 1998;218:8–14.
[39] Kikuchi N, Kitagawa M, Sato A, Kusano E, Nanto H, Kinbara A. Surf Coat Technol 2000;126:131–5.
[40] Field JE, Telling RH. The Young's modulus and Poisson ratio of diamond. Research Note, PCS Cavendish Laboratory, Department of Physics, Cambridge CB3 0HE, UK, February 1999.
[41] Hainsworth SV, Chandler HW, Page TF. J Mater Res 1996;11:1987.
[42] Zeng K, Rowcliffe D. Phil Mag A 1996;74:1107.
[43] Cheng Y-T, Cheng C-M. Appl Phys Lett 1998;73:614.
[44] Malzender J, de With G, den Toonder JMJ. J Mater Res 2000;15:1209–12.
[45] Hayes NW, Beamson G, Clark DT, Law DS-L, Raval R. Surf Interf Anal 1996;24:723.
[46] Chudoba, T., Richter, F., 2001, in press.
[47] Beake BD, Gao F, Chen S. Unpublished work.
[48] Johnson SA. Nanoindentation and nanoscratch testing of organic coatings. London: UK Coatings Forum, 2001.
[49] den Toonder JMJ. Personal communication.
[50] Gao F. Personal communication.
[51] Beake BD, Leggett GJ, Shipway PH. Unpublished work.